Subterahertz Momentum Drag and Violation of Matthiessen's Rule in an Ultraclean Ferromagnetic SrRuO₃ Metallic Thin Film

Youcheng Wang[1], G. Bossé,[1,2] H. P. Nair,[3] N. J. Schreiber,[3] J. P. Ruf[4], B. Cheng,[1] C. Adamo,[3] D. E. Shai,[4]
Y. Lubashevsky,[1] D. G. Schlom[3,5] K. M. Shen,[4,5] and N. P. Armitage[1]

[1]*The Institute for Quantum Matter, Department of Physics and Astronomy, The Johns Hopkins University,
Baltimore, Maryland 21218, USA*
[2]*Physics Department, University of North Florida, Jacksonville, Florida 32224-7699, USA*
[3]*Department of Materials Science and Engineering, Cornell University, Ithaca, New York 14853, USA*
[4]*Laboratory of Atomic and Solid State Physics, Department of Physics, Cornell University, Ithaca, New York 14853, USA*
[5]*Kavli Institute at Cornell for Nanoscale Science, Ithaca, New York 14853, USA*

SrRuO₃, a ferromagnet with an approximately 160 K Curie temperature, exhibits a T^2-dependent dc resistivity below ≈ 30 K. Nevertheless, previous optical studies in the infrared and terahertz range show non-Drude dynamics at low temperatures, which seem to contradict Fermi-liquid predictions. In this work, we measure the low-frequency THz range response of thin films with residual resistivity ratios, $\rho_{300K}/\rho_{4K} \approx 74$. At temperatures below 30 K, we find both a sharp zero frequency mode which has a width narrower than $k_B T/\hbar$ as well as a broader zero frequency Lorentzian that has at least an order of magnitude larger scattering. Both features have temperature dependences consistent with a Fermi liquid with the wider feature explicitly showing a T^2 scaling. Above 30 K, there is a crossover to a regime described by a single Drude peak that we believe arises from strong interband electron-electron scattering. Such two channel Drude transport sheds light on reports of the violation of Matthiessen's rule and extreme sensitivity to disorder in metallic ruthenates.

The 4d ruthenates are well suited to the study of itinerant correlated electrons and the stability of the Fermi-liquid state because no explicit doping is necessary to produce metallic conduction [1–5]. The position of the Fermi level in bands resulting from the hybridization of O 2p and Ru 4d leads to ground-state behavior ranging from ferromagnetism in SrRuO₃, metallic paramagnetism in CaRuO₃ [6], insulating antiferromagnetism in Ca₂RuO₄, quantum critical metamagnetism in Sr₃Ru₂O₇ [7], and unconventional superconductivity in Sr₂RuO₄ [5]. These materials present an opportunity to investigate correlated electrons in the low-disorder limit.

SrRuO₃ exhibits a transition from a paramagnetic to a ferromagnetic state at $T_c \approx 160$ K. Quantum oscillations and a quadratic temperature dependence of the resistivity have been measured in the highest-quality samples [4,8]. These findings suggest that the ground state of SrRuO₃ is a magnetic Fermi liquid. Anomalous Hall and magneto-optical measurements suggest the existence of intrinsic Berry phase effects near the Fermi energy [9,10]. Nevertheless, among other experimental observations, infrared and optical measurements of SrRuO₃ films (that generally have had higher-disorder levels than single crystals) have shown a finite frequency peak in σ_1 at frequencies of order $3k_B T$ [11]. At frequencies above the peak, the real part of the optical conductivity was observed to fall off as $\omega^{-1/2}$ [11].

Optical measurements at lower frequency gave evidence for a related fractional power law dependence of the conductivity on the transport relaxation time [12]. The theoretical basis to understand this seeming deviation from the Lorentzian Drude form (and by implication the non-Fermi-liquid nature of this material) is not clear considering the radical implications it would have on the link between ac and dc electrical transport. Similar deviations from simple Drude forms of finite frequency peaks and anomalous power laws have been seen in the related compound CaRuO₃ [6,13]. In addition, SrRuO₃ has a very striking negative deviation from Matthiessen's rule when impurity scattering is increased through electron irradiation. It was demonstrated that although the fractional form works for more disordered samples, it does not account for this violation for low-disorder samples [14,15]. These results highlight the extreme sensitivity to disorder in this material and the apparent dependence of even the inelastic scattering on sample quality. Therefore, measuring low-disorder SrRuO₃ samples at low energies would provide a unique opportunity to examine Fermi-liquid predictions in this strongly correlated material. Previous studies were performed at higher frequencies and/or on samples with larger disorder. Recently, extremely low-disorder films were grown of which photoemission measurements reveal a complement of heavy low energy bands [16].

In this Letter, we use time domain terahertz spectroscopy (TDTS) to examine the complex conductivity and resistivity of very-high-quality thin films of SrRuO$_3$. Below 30 K, we find the real part of the THz conductivity exhibits two very distinct low energy peaks that are related to different conduction channels. There is both a very sharp zero frequency conducting mode which has a width narrower than $k_B T/\hbar$ as well as a broader Lorentzian peak with at least an order of magnitude larger scattering rate. Both features have temperature dependences consistent with a Fermi liquid with the wider feature explicitly showing a T^2 scaling. There are a number of possibilities for the origin of these features including multiband effects that arise from momentum conserving interband scattering and the approximate conservation of a pseudomomentum that arises from this material's quasi-1D Fermi surface sheets. Above 30 K, there is a crossover to a regime described by a single Drude peak that we believe arises from strong interband electron-electron scattering.

In TDTS, an approximately 1 ps long electromagnetic pulse is transmitted through a substrate and film. The complex transmission $T(\omega)$ is obtained from the Fourier transform of the time trace referenced to a bare substrate. Complex conductivity $\sigma(\omega)$ is calculated without the need for Kramers-Kronig transformation from the complex transmission using $T(\omega) = [(1+n)/1 + n + \sigma(\omega)dZ_0]e^{[(i\omega\Delta L(n-1))/(c)]}$. In this expression, n is the substrate index, ΔL is a correction that accounts for thickness differences between the reference substrate and the sample substrate, d is the film thickness, and Z_0 is the impedance of free space (377 Ω). We determined the effective ΔL from a self-consistent first echo measurement of the sample and substrate at different temperatures. The proper determination of ΔL to submicron accuracy is essential for the accuracy of these results [17]. The films were grown on single-crystal DyScO$_3$ (110) substrates by molecular-beam epitaxy to a thickness of 23 nm [17]. Because this substrate is very lossy to the THz signal in the [001] direction (see Supplemental Material [17] Fig. S3), in all presented measurements the polarization of the incident THz beam is aligned parallel to the [$\bar{1}$10] direction. Our data on samples grown on less lossy (and more highly strained) NdGaO$_3$ substrates show that the in-plane anisotropy is less than 20% with no qualitative difference between the two directions (Supplemental Material [17] Fig. S4).

dc resistivity $\rho(T)$ was measured in the van der Pauw geometry and anisotropy determined from the Montgomery method [28] [Fig. 1(a)]. The kink at 168 K is attributed to the development of ferromagnetic order [29]. The high quality of the film is reflected in its low residual resistivity of $\rho(T \to 0) \sim 2.6\ \mu\Omega$ cm giving a large residual resistivity ratio of ≈ 74 along the [$\bar{1}$10] direction. This residual resistivity is almost 20 times lower than the films used in previous TDTS studies [12]. A quadratic dependence on the temperature of $\rho(T) - \rho(0)$ has been reported up to at least 30 K [inset of Fig. 1(a)]. Our observation of a T^2
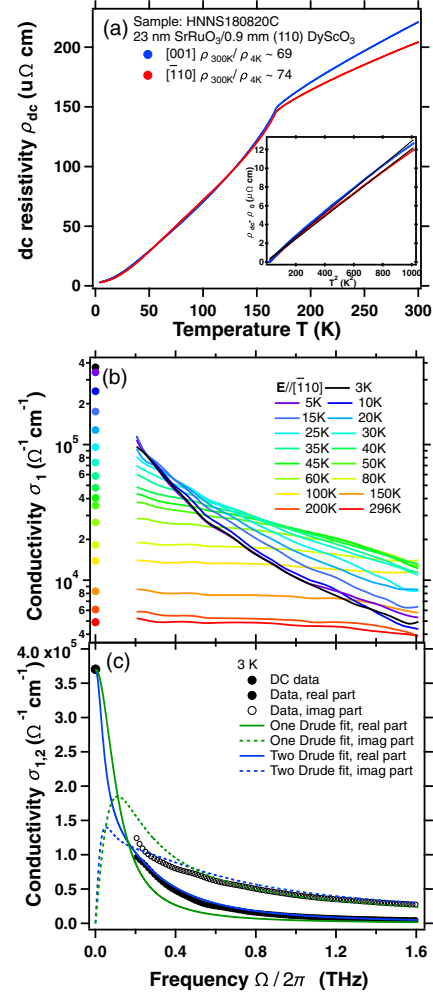

FIG. 1. (a) dc resistivity as a function of the temperature for the SrRuO$_3$ film for the two orthogonal directions. Inset: resistivity minus residual resistivity as a function of T^2. Fits to the data in the temperature range 2–32 K are shown as black lines. (b) Real part of the THz conductivity σ_1 from 5 K to room temperature along with corresponding dc values. (c) One Drude vs two Drude fit of dc and THz data at 3 K. The dc conductivity and real and imaginary parts of the complex conductivity are fitted simultaneously.

dependence of the resistivity is consistent with other studies on low-disorder samples [8,30] as opposed to behavior T^β, where $\beta \sim 1$–2 is observed primarily in samples with residual resistivities above 50 $\mu\Omega$ cm [29].

In Fig. 1(b), we plot the real part of the THz and dc conductivity at different temperatures. With decreasing temperature, there is a remarkable sharpening of a low-frequency Drude-like peak. The real σ_1 and imaginary σ_2 parts of the complex conductivity, with corresponding dc values at 3 K are plotted in Fig. 1(c). At this temperature, the peak in σ_1 is so narrow that $\sigma_2 > \sigma_1$ for the entire frequency range measured. In a simple single-band metal, one expects that the scattering of electrons is dominated by quenched disorder as $T \to 0$ and that the dynamical
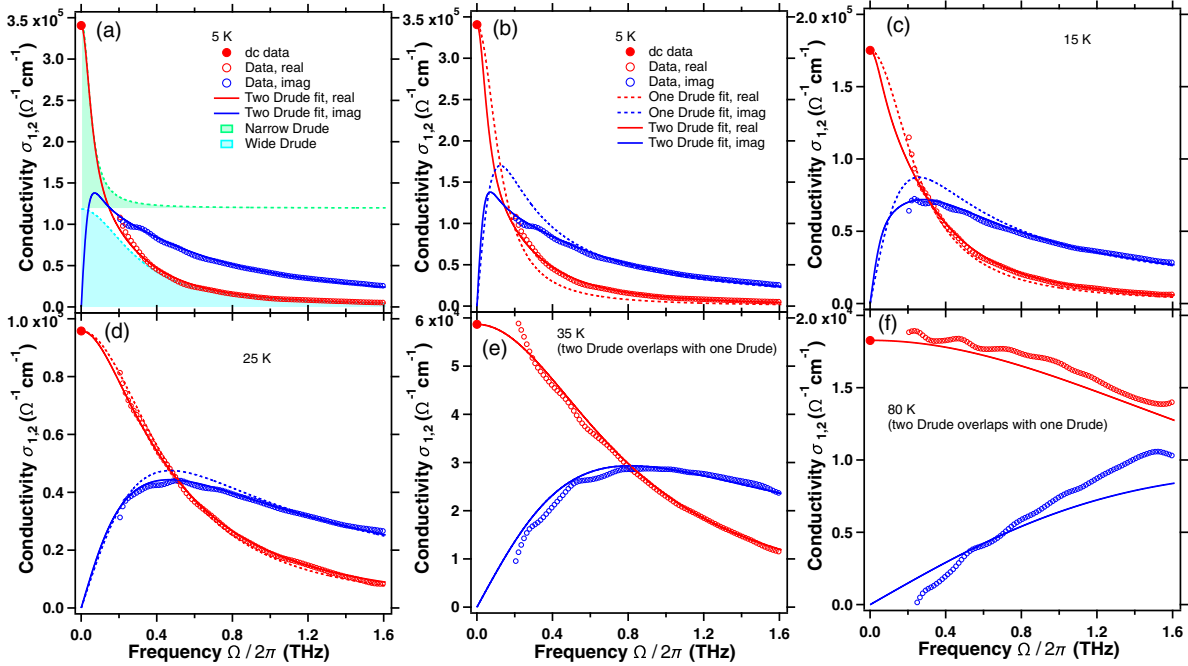
FIG. 2. (a) Real and imaginary THz conductivity with dc values at 5 K. The red and blue solid lines show fitting with two Drude terms. The green and blue shaded regions correspond to a narrow and wider Drude term, respectively. The green shade is offset to distinguish from the other. (b)–(f) Real and imaginary parts of the complex conductivity with dc values for 5 K [same data as in (a)], 15, 25, 35, and 80 K. The data are presented with one Drude (dashed lines) and two Drude modeling (solid lines). Note that for 35 and 80 K, two Drude terms from fitting have the same scattering rates, so the two Drude overlaps with one Drude fitting. In (b)–(f) the same line types are used.

conductivity can be modeled with a single Drude oscillator with the functional form $\sigma(\omega) = \epsilon_0[(\omega_p^2)/(1/\tau - i\omega)]$ (where ω_p is the plasma frequency and $1/\tau$ is the current decay rate). Although the σ_1 data superficially have such a Drude form, the 3 K complex conductivity, in fact, cannot be reproduced with a single Drude oscillator. As can be seen in Fig. 1(c), the best fits with a single Drude oscillator to the THz constrained with the dc resistivity underestimates the real conductivity and overestimates the imaginary conductivity. Note that we can make such an assessment despite the fact that the spectral range between dc and 200 GHz is not measured because the real and imaginary parts of σ are Kramers-Kronig related to each other; e.g., the data are strongly constrained for parts of the spectral range that are not explicitly measured, by parts that are measured. In order to fit the 3 K conductivity, at least two Lorentzian oscillators are needed: one narrow with $1/\tau_1 \lesssim 50$ GHz scattering rate and one wider with $1/\tau_2 \sim 300$ GHz scattering rate. Because the narrow oscillator has a width below the measured frequency range, we can only set an upper limit on its width, although we are highly sensitive to its spectral weight. In these fits, we adopt the highest value of $1/\tau_1$ consistent with THz data as its upper bound. The full functional form is $\sigma(\omega) = \sum_{n=1}^2 \epsilon_0 \omega_{p_n}^2 [1/(1/\tau_n - i\omega)] - i\epsilon_0(\epsilon_\infty - 1)\omega$. ϵ_∞ accounts for effects of interband transitions at frequencies well above our range. As discussed below, the appearance

of multiple Lorentzian Drude peaks is a natural expectation for a multiband metal.

The necessity to use two Drude terms extends to higher temperatures. One can see in the 5 K conductivity [Fig. 2(a)] that the narrow Drude (green area under the real part of the narrow Drude) accounts for the sharp upturn toward the dc conductivity, whereas the wide Drude part (blue) is needed to capture the long tail of $\sigma_1(\omega)$. In the data up to 30 K [Figs. 2(b) and 2(c)], one cannot fit the imaginary part of the conductivity with a single Drude if one insists on a fit of the real part. As the temperature increases, the scattering rate of the narrow Lorentzian increases faster than the scattering rate of the wider one, and the rates become equal above 30 K and the Lorentzians indistinguishable. Hence, a single Drude fitting above 30 K suffices. It is interesting to note that this temperature is close to that below which T^2 resistivity has been reported. The scattering rate of the wide Drude peak goes as T^2 below 30 K. The total spectral weight [Fig. 3(b)] is unchanged within 5% below 30 K, while the narrow Drude peak corresponds to about 20% of the total weight in the range where it can be distinguished. Note that the fractional functional form used previously [12] does not fit our data (Supplemental Material [17] Sec. IV). Also note that we see no sign of meV range finite frequency peaks arising from either finite temperature effects as observed previously in higher-disorder samples [11] or
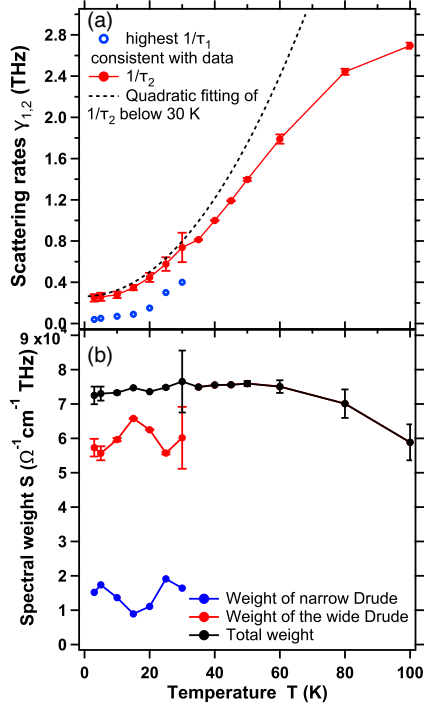
FIG. 3. (a) Scattering rate of the wide (red) and narrow (blue) Drude peaks as a function of T. The dashed line is a quadratic fit to the data below 30 K, and extended to higher T. (b) Spectral weight of the two Drude peaks (obtained from two Drude fitting) and their total spectral weight, from 5 to 30 K. Above 30 K, single Drude fit parameters are given. The spectral weight is proportional to ω_p^2.

that have been predicted to arise from the tilt of the octahedra [31].

We examined complex resistivity which is the inverse of complex conductivity data [17]. For a single-band metal, the "Gurzhi" scaling [32] for a metal with dominant umklapp scattering as $T \rightarrow 0$ predicts the real part of the resistivity goes as $\rho_1(T, \omega) = \rho_0^{ee}(T)[1 + (\hbar\omega)^2/b\pi^2(k_BT)^2]$ where $\rho_0^{ee}(T)$ is the quadratic dc resistivity. This relation arises from the established relation between T- and ω-induced inelastic scattering [33]. With the b that is predicted to be 4 for a canonical Fermi liquid, the scattering is dominated in our temperature and frequency range by the temperature; e.g., the broadening at 30 K at zero frequency is expected to be approximately 16.6 times larger than the broadening at 1 THz at $T = 0$. This is consistent with our data in that we find very little frequency-dependent changes to ρ_1 (Supplemental Material [17] Figs. S6 and S7), while the T-dependence changes are large. When intraband scattering processes dominate, the complex resistivity can be related to the "extended" Drude model (EDM), in which the scattering rate and effective masses in the Drude formula become complex and frequency dependent [34]. The EDM has been used extensively to describe heavy fermion systems [35,36], high-T_c cuprates [2], and transition-metal

compounds [37]. Within the context of EDM, the slope of the imaginary part of the complex resistivity with frequency is proportional to the optical renormalized mass (m^*/m_b; m_b is the effective band mass). It is found that in our TDTS data, mass enhancement at the lowest temperatures is ~ 6.5 [Supplemental Material [17] Fig. S6(b)], which roughly agrees with heat capacity and de Haas–van Alphen measurements [29,38]. In particular, heat capacity measurements show a Sommerfeld coefficient $\gamma_{\text{expt}}/\gamma_{\text{theor}} = 3.7$, suggesting a mass enhancement similar to what we observe in TDTS measurements [29]. According to an angle-resolved de Haas–van Alphen study, the effective mass of charge carriers measured for each Fermi surface sheet ranges from 4.1 to $6.9m_e$ [38]. Similarly, angle-resolved photoemission has found masses of order $3.7m_e$ [16] for the β sheet.

We now discuss the possible origins of the multiple low-frequency Drude peaks and the crossover to a single peak at higher temperature. As mentioned above, one expects in a multiband metal like $SrRuO_3$ a number of independent conduction channels. In the low-temperature limit, disorder scattering is expected to be dominant, and the different channels will manifest as different Lorentzian Drude peaks. These may have very different residual widths as the rate of scattering by short-range impurities is proportional to the density of states of the band, which may be very different between bands. At high temperatures, electron-electron scattering will dominate. In an almost compensated metal such as $SrRuO_3$, scattering serves to equalize net velocities between electrons and hole bands giving rise to a single Drude peak [33,39]. This crossover scenario is quite general and discussed in more detail in the Ref. [17]. In a different scenario, Rosch and Andrei have shown [40,41] that in 1D it is possible to define a pseudomomentum that does not decay by two-particle collisions and hence decays more slowly than the conventional crystal momentum. It is expected that a state with finite pseudomomentum has significant projection on current-carrying states. This gives rise to well-defined and sharp peaks in the optical conductivity. One might expect these effects in even quasi-2D metals like $SrRuO_3$ as its Fermi surface is composed of primarily 1D sections that show only weak hybridization where the bands intersect. Irrespective of the mechanism, what these scenarios share is the idea that scattering channels *add* in the conductivity not the resistivity. The latter is the usual Matthiessen rule, and in this regard, our results give understanding of the deviations from Matthiessen's rule in this material.

We have examined THz dynamical conductivity in clean films of $SrRuO_3$, which have more than an order of magnitude smaller residual resistivity than previously measured samples, and observed very different results. At low temperature, a narrow Drude-like peak emerges, which cannot be parametrized with a single oscillator. As it is the low-frequency and low-temperature properties of a

system which are diagnostic of its ground state, the T^2 dependence of the widths of the low energy conductivity peaks confirm the Fermi-liquid nature of this compound. The presence of multiple Drude peaks, however, indicates effects beyond conventional Boltzmann transport and might help explain previous reports of deviations from Matthiessen's rule. They may indicate either the presence of extremely strong momentum-conserving electron-electron interactions or an almost conserved pseudomomentum due to quasi-1D Fermi surfaces of this system.

[1] G. Koster, L. Klein, W. Siemons, G. Rijnders, J. S. Dodge, C.-B. Eom, D. H. A. Blank, and M. R. Beasley, Rev. Mod. Phys. **84**, 253 (2012).

[2] A. V. Puchkov, D. N. Basov, and T. Timusk, J. Phys. Condens. Matter **8**, 10049 (1996).

[3] Y. Maeno, Physica (Amsterdam) **282C–287C**, 206 (1997).

[4] L. Capogna, A. P. Mackenzie, R. S. Perry, S. A. Grigera, L. M. Galvin, P. Raychaudhuri, A. J. Schofield, C. S. Alexander, G. Cao, S. R. Julian *et al.*, Phys. Rev. Lett. **88**, 076602 (2002).

[5] R. S. Perry, L. M. Galvin, S. A. Grigera, L. Capogna, A. J. Schofield, A. P. Mackenzie, M. Chiao, S. R. Julian, S. Ikeda, S. Nakatsuji, Y. Maeno, and C. Pfleiderer, Phys. Rev. Lett. **86**, 2661 (2001).

[6] S. Kamal, D. M. Kim, C. B. Eom, and J. S. Dodge, Phys. Rev. B **74**, 165115 (2006).

[7] S. Grigera, R. Perry, A. Schofield, M. Chiao, S. Julian, G. Lonzarich, S. Ikeda, Y. Maeno, A. Millis, and A. Mackenzie, Science **294**, 329 (2001).

[8] A. P. Mackenzie, J. W. Reiner, A. W. Tyler, L. M. Galvin, S. R. Julian, M. R. Beasley, T. H. Geballe, and A. Kapitulnik, Phys. Rev. B **58**, R13318 (1998).

[9] Z. Fang, N. Nagaosa, K. S. Takahashi, A. Asamitsu, R. Mathieu, T. Ogasawara, H. Yamada, M. Kawasaki, Y. Tokura, and K. Terakura, Science **302**, 92 (2003).

[10] N. Hosaka, H. Yamada, Y. Shimada, J. Fujioka, S. Bordács, I. Kézsmárki, M. Kawasaki, and Y. Tokura, Appl. Phys. Express **1**, 113001 (2008).

[11] P. Kostic, Y. Okada, N. C. Collins, Z. Schlesinger, J. W. Reiner, L. Klein, A. Kapitulnik, T. H. Geballe, and M. R. Beasley, Phys. Rev. Lett. **81**, 2498 (1998).

[12] J. S. Dodge, C. P. Weber, J. Corson, J. Orenstein, Z. Schlesinger, J. W. Reiner, and M. R. Beasley, Phys. Rev. Lett. **85**, 4932 (2000).

[13] Y. S. Lee, J. Yu, J. S. Lee, T. W. Noh, T.-H. Gimm, H.-Y. Choi, and C. B. Eom, Phys. Rev. B **66**, 041104(R) (2002).

[14] L. Klein, Y. Kats, N. Wiser, M. Konczykowski, J. Reiner, T. Geballe, M. Beasley, and A. Kapitulnik, Europhys. Lett. **55**, 532 (2001).

[15] Y. Kats and L. Klein, Physica (Amsterdam) **312B–313B**, 793 (2002).

[16] D. E. Shai, C. Adamo, D. W. Shen, C. M. Brooks, J. W. Harter, E. J. Monkman, B. Burganov, D. G. Schlom, and K. M. Shen, Phys. Rev. Lett. **110**, 087004 (2013).

[17] See Supplemental Material at http://link.aps.org/supplemental/10.1103/PhysRevLett.125.217401 Sec. II for details about the measurement of δ_L, which includes Ref. [18], for the extended Drude analysis, which includes Refs. [19,20], and for the attempts to measure the microwave conductivity, which includes Refs. [21,22]. Section I for details about sample growth, which includes Refs. [23–25]. Section VII for the modeling of the conductivity of a two-band metal, which includes Refs. [26,27].

[18] A. B. Sushkov, G. S. Jenkins, D. C. Schmadel, N. P. Butch, J. Paglione, and H. D. Drew, Phys. Rev. B **82**, 125110 (2010).

[19] I. I. Mazin and D. J. Singh, Phys. Rev. B **56**, 2556 (1997).

[20] I. I. Mazin and D. J. Singh, Phys. Rev. B **73**, 189903(E) (2006).

[21] W. Liu, Ph.D. Thesis, The Johns Hopkins University, 2013.

[22] M. Scheffler, S. Kilic, and M. Dressel, Rev. Sci. Instrum. **78**, 086106 (2007).

[23] H. P. Nair, Y. Liu, J. P. Ruf, N. J. Schreiber, S.-L. Shang, D. J. Baek, B. H. Goodge, L. F. Kourkoutis, Z.-K. Liu, K. M. Shen *et al.*, APL Mater. **6**, 046101 (2018).

[24] D. B. Kacedon, R. A. Rao, and C. B. Eom, Appl. Phys. Lett. **71**, 1724 (1997).

[25] F. Chu, Q. Jia, G. Landrum, X. Wu, M. Hawley, and T. Mitchell, J. Electron. Mater. **25**, 1754 (1996).

[26] P. F. Maldague and C. A. Kukkonen, Phys. Rev. B **19**, 6172 (1979).

[27] W. G. Baber, Proc. R. Soc. A **158**, 383 (1937).

[28] H. Montgomery, J. Appl. Phys. **42**, 2971 (1971).

[29] P. B. Allen, H. Berger, O. Chauvet, L. Forro, T. Jarlborg, A. Junod, B. Revaz, and G. Santi, Phys. Rev. B **53**, 4393 (1996).

[30] G. Cao, O. Korneta, S. Chikara, L. DeLong, and P. Schlottmann, Solid State Commun. **148**, 305 (2008).

[31] H. T. Dang, J. Mravlje, A. Georges, and A. J. Millis, Phys. Rev. Lett. **115**, 107003 (2015).

[32] R. N. Gurzhi, Sov. Phys. JETP **8**, 673 (1959), http://www.jetp.ac.ru/cgi-bin/dn/e_008_04_0673.pdf.

[33] D. L. Maslov and A. V. Chubukov, Rep. Prog. Phys. **80**, 026503 (2017).

[34] D. N. Basov and T. Timusk, Rev. Mod. Phys. **77**, 721 (2005).

[35] B. C. Webb, A. J. Sievers, and T. Mihalisin, Phys. Rev. Lett. **57**, 1951 (1986).

[36] L. Degiorgi, Rev. Mod. Phys. **71**, 687 (1999).

[37] J. W. Allen and J. C. Mikkelsen, Phys. Rev. B **15**, 2952 (1977).

[38] C. S. Alexander, S. McCall, P. Schlottmann, J. E. Crow, and G. Cao, Phys. Rev. B **72**, 024415 (2005).

[39] V. Gantmakher and Y. Levinson, *Modern Problems in Condensed Matter Sciences Vol. 19: Carrier Scattering in Metals and Semiconductors* (Elsevier–North-Holland, New York 1987).

[40] A. Rosch and N. Andrei, J. Low Temp. Phys. **126**, 1195 (2002).

[41] A. Rosch, Ann. Phys. (Amsterdam) **15**, 526 (2006).

Supplemental Material: Sub-THz momentum drag and violation of Matthiessen's rule in an ultraclean ferromagnetic SrRuO$_3$ metallic thin film

Youcheng Wang[1], G. Bossé[1,2], H. P. Nair[3], N. J. Schreiber[3], J. P. Ruf[4], B. Cheng[1], C. Adamo[3], D. E. Shai[4], Y. Lubashevsky[1], D. G. Schlom[3,5], K. M. Shen[4,5], and N. P. Armitage[1]

[1] The Institute for Quantum Matter, Department of Physics and
Astronomy, The Johns Hopkins University, Baltimore, MD 21218 USA
[2] Physics Department, University of North Florida, Jacksonville, FL 32224-7699, USA
[3] Department of Materials Science and Engineering, Cornell University, Ithaca, New York 14853, USA
[4] Laboratory of Atomic and Solid State Physics, Department
of Physics, Cornell University, Ithaca, New York 14853, USA
[5] Kavli Institute at Cornell for Nanoscale Science, Ithaca, New York 14853, USA
(Dated: August 13, 2020)

I. EXPERIMENTAL DETAILS

The SrRuO$_3$ thin films studied in this work were grown on single-crystal (110) DyScO$_3$ substrates by molecular-beam epitaxy (MBE) in a dual chamber Veeco GEN10 system to a thickness of $\sim$23 nm[1]. Adsorption-controlled growth conditions are used in which an excess flux of elemental ruthenium is supplied to the growing film and thermodynamics controls its incorporation through the desorption of volatile RuOx. This growth regime minimizes ruthenium vacancies in the films and the resulting samples exhibit a high residual resistivity ratio (RRR) in transport measurements[1]. The strong dependence of spectral features on sample quality highlights the necessity for such studies of utilizing oxide MBE, which produces higher quality films than those grown by pulsed laser deposition or sputtering[1–3].

In the technique of TDTS an infrared femtosecond laser pulse is split between two paths and excites a pair of "Auston" switch photoconductive antennae; one acts as an emitter and the other acts as a receiver. When the laser pulse hits the voltage-biased emitter, a broadband terahertz pulse is produced and collimated by mirrors and lenses and passes through the sample. The terahertz pulse then falls on the receiving Auston switch. Current only flows across the receiver switch at the instant the other short femtosecond pulse impinges on it. By varying the difference in path length between the two pulses, the entire electric field of the transmitted pulse can be mapped out as a function of time. By dividing the Fourier transform of transmission through the sample by the Fourier transform of transmission through a reference substrate, one obtains the full complex transmission $T(\omega)$ over a frequency range that can be as broad as 100 GHz to 3.5 THz. The complex transmission is used to calculate the complex conductivity $\sigma(\omega)$ without the need for Kramers-Kronig transformation using the expression $T(\omega) = \frac{(1+n)}{1+n+\sigma(\omega)dZ_0}e^{\frac{i\omega\Delta L(n-1)}{c}}$. In this expression n is the index of refraction of the substrate, ΔL is a correction factor that accounts for thickness difference between the reference substrate and the sample substrate, d is the film thickness, and Z_0 is the impedance of free space (377 Ω). ΔL is a correction to the phase of complex transmission and thus also the complex conductivity. We determined the effective ΔL from a self-consistent measurement of the first echo of the sample and substrate at different temperatures (see Supplemental Material Section II below).

II. ΔL DETERMINATION

The thickness difference between the sample substrate and a reference substrate, i.e., ΔL, is usually on the order of a few microns. Its correct determination can greatly effect the phase of calculated conductivity. A rough measurement can be made by using a micrometer on the corners of the samples, but the thickness at the center where the optical aperture is at might be different from the corners. Here we use a self-consistent measurement of the first echo of the time domain pulse to determine the value of ΔL precisely.

The measurement was performed by taking extended scans in time in which the transmitted THz pulse and the first echo pulse (e.g., the time delayed pulse that comes from internal reflections inside the substate) are included, for both the sample and the bare substrate. The phase accumulation can be modeled as in Fig. S1. Here A_i and B_i are complex phase winding in the optical path in medium i. T_{ij} and R_{ij} are the phase shifts coefficients of transmission and reflection from the interface of medium i and j, as determined from Fresnel equations. Fig. S2(a) shows time scans of the pulses at 5 K. The transmitted and first echo pulse of the same duration ($\sim$ 20 ps) are cut from the data and then Fourier transformed, for the sample and substrate respectively. The Fourier transform of the first echo is divided by the Fourier transform of the transmitted pulse (see equations in Fig. S1). This is done for the substrate
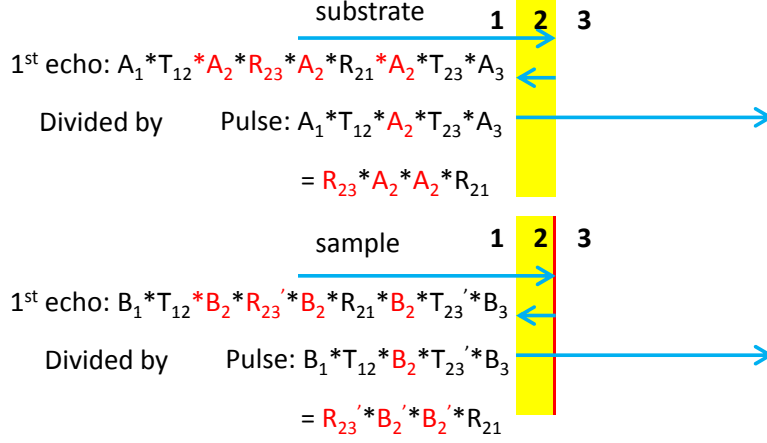
substned (substrate)   1 **2** 3

1st echo: $A_1*T_{12}*A_2*R_{23}*A_2*R_{21}*A_2*T_{23}*A_3$

Divided by   Pulse: $A_1*T_{12}*A_2*T_{23}*A_3$

$= R_{23}*A_2*A_2*R_{21}$

sample   1 **2** 3

1st echo: $B_1*T_{12}*B_2*R_{23}^{'}*B_2*R_{21}*B_2*T_{23}^{'}*B_3$

Divided by   Pulse: $B_1*T_{12}*B_2*T_{23}^{'}*B_3$

$= R_{23}^{'}*B_2^{'}*B_2^{'}*R_{21}$

FIG. 1: Phase accumulation in a first echo measurement. The blue arrows indicate the propagation of THz pulse. 1, 2, and 3 corresponds to vacuum, $DyScO_3$ and vacuum in this case. The red vertical line represents the thin film sample. Details about the symbols are explained in the text.

and sample respectively. The result for the sample is divided by the result of the substrate which is then, according to the equations in Fig. S1. While R_{21} cancels, R_{23} and $R_{23}^{'}$ are different which are given by Fresnel's equations (for example, see[4])

$$R_{23} = \frac{n_2 - n_3}{n_2 + n_3} \; ; R_{23}^{'} = \frac{n_2 - n_3 - y_s}{n_2 + n_3 + y_s} \tag{1}$$

Here n_2 and n_3 are the indices of refraction for $DyScO_3$ (which we measure separately by referencing to an empty aperture) and vacuum, and y_s is the admittance of the sample normalized with respect to $1/376.73 \; \Omega$ (the admittance of vacuum). Since the admittance of the sample relies on the value of Δ_L it has to be determined through iteration until convergence (see below). The phase difference coming from the remaining factors are associated with Δ_L as in the following equation

$$\Delta\Phi = 2\omega\Delta L \frac{n}{c} \tag{2}$$

Therefore if after subtracting off the phase factors calculated from Eq. 1 one fits the phase versus frequency to a straight line (see Fig. S2(b)) the slope is proportional to ΔL with known or measured factors/functions including speed of light and the measured index of refraction of the substrate. Typically one starts with an initial guess coming from micrometer measurements say a few microns and calculate the conductivity and use this as input for the admittance to calculate $R_{23}^{'}$ to obtain a new value of ΔL. This process is repeated for each temperature until convergence. For this sample/substrate combination ΔL converges to about 12.5 μm for both 5 K and 100 K.

III. OPTICAL ANISOTROPY

As discussed in the main text, the orthorhombic $DyScO_3$ substrate has larger optical absorptions for light polarized along the $\langle 001 \rangle$ axis than the $\langle -110 \rangle$ axis. See Fig. S3(a), which shows a comparison of the magnitude of room temperature transmission $T(\omega)$ along these two orthogonal directions. One can see there is little signal above 0.8 THz for polarizations along $< 001 >$ axis, possibly owing to the strong absorption by polarized phonons in this frequency range. When one divides the FFT of the time trace of sample pulse by reference pulse one gets very noisy data above 0.8 THz as shown in Fig. 3(b)). This makes data taken with $\langle 001 \rangle$ polarized light unreliable for this substrate.

However, a comparison with samples grown on the $NdGaO_3$ substrate shows that anisotropy of $SrRuO_3$ is likely intrinsically weak. A sample of ~ 20 nm in thickness has a RRR of around 20. One can see from the 5 K data (Fig. S4) that there is no qualitative difference between the two directions. Both conductivities are Drude-like in shape with slightly different scattering rates.
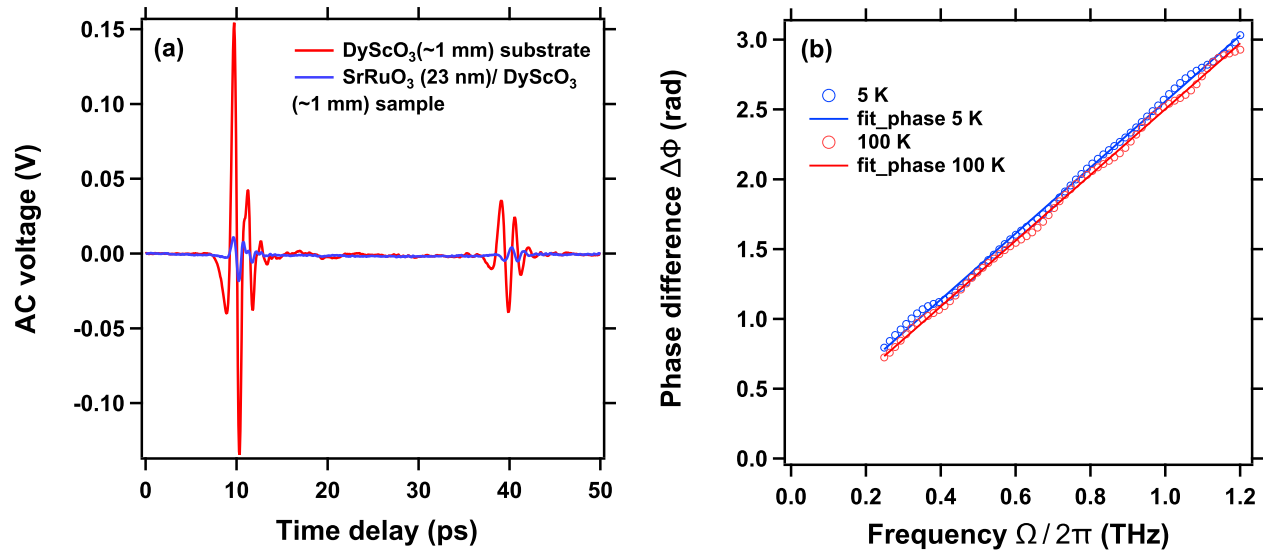
FIG. 2: (a) Measured time traces of the sample (blue) and substrate (red) pulses at 5 K. (b) Linear fits to the calculated phase difference between substrate and sample as a function of frequency. Data were taken at two temperatures and the obtained Δ_L were interpolated in between.
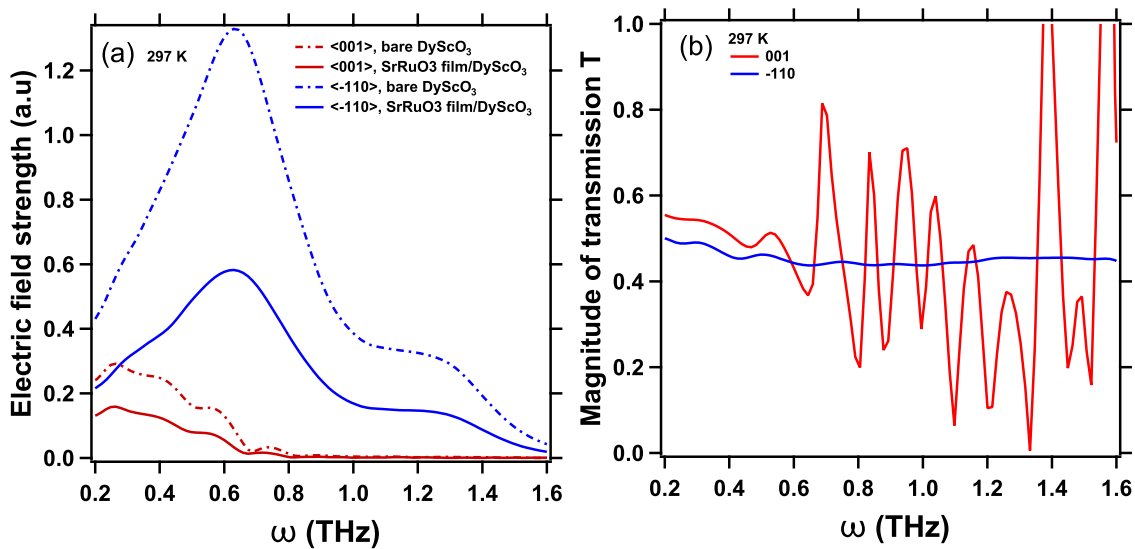

FIG. 3: (a) The electric field strength as a function of frequency, through reference substrate and thin film (with substrate) along two directions. The data shown are FFTs of the time domain traces. (b) The magnitude of transmission of the sample at room temperature along two orthogonal crystallographic axes.

IV. FRACTIONAL FUNCTIONAL FORM

Previous work[5] on the THz conductivity of $SrRuO_3$ used an expression of the form

$$\sigma(\omega) = \frac{A}{(1/\tau - i\omega)^\alpha} \tag{3}$$

to fit the conductivity data using $\alpha = 0.4$. Although excellent fits were obtained, this was a radical proposal considering the implications it would have on the link between ac and dc electrical transport measurements. Moreover its microscopic basis in the context of $SrRuO_3$ was not clear. In our case, we cannot simultaneously fit both the magnitude and phase of the measured conductivity using this functional form. This can be readily seen from Fig.
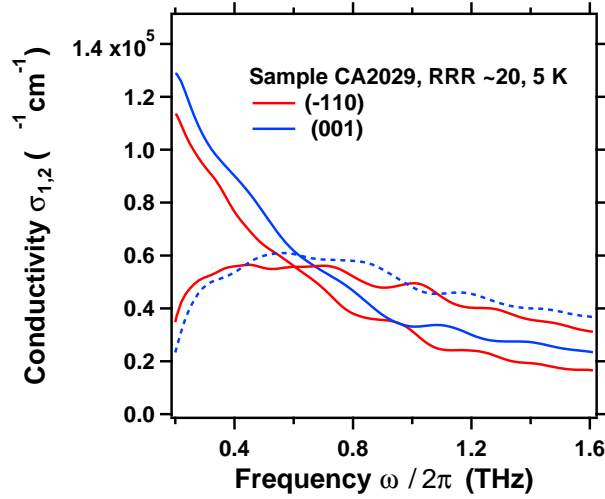
FIG. 4: The room temperature conductivity of a sample grown on NdGaO$_3$ along two orthogonal crystallographic axes. One can see the anisotropy is weak.
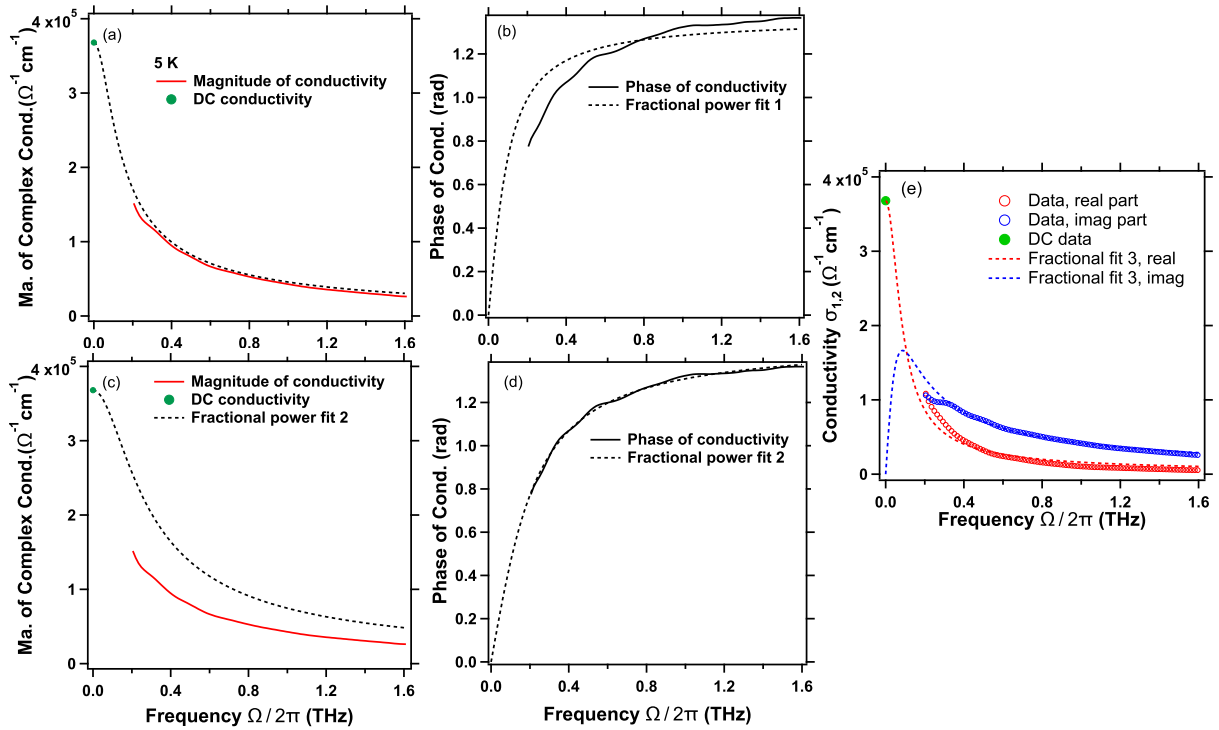

FIG. 5: Fits of 5K conductivity data to Eq. 3. (a) and (b). A good fit to the magnitude is possible only if the fit to the phase is disregarded. Here $1/\tau = 80.9$ GHz and $\alpha = 0.853$. (c) and (d) A good fit to the magnitude is possible only if the magnitude is disregarded. Here $1/\tau = 0.189$ THz and $\alpha = 0.946$. (e) A fit by converting to real and parts of the fractional power formula, with equal weights assigned to either part. Here $1/\tau = 72.8$ GHz and $\alpha = 0.803$.

S5. A good fit to the magnitude is possible only if the fit to the phase is disregarded (Fig. S5(a-b)). In this case $1/\tau$ = 80.9 GHz and $\alpha = 0.853$. A good fit to the phase is possible only if the magnitude is disregarded (Fig. S5(c-d)). In this case $1/\tau = 0.189$ THz and $\alpha = 0.946$. An alternative fit is done by converting the fractional formula from magnitude and phase to the real and imaginary basis, and assigning equal weight to them (Fig. S5(e)). In this case, $1/\tau = 72.8$ GHz and $\alpha = 0.803$. Note that in none of these cases is the α exponent close to the 0.4 found in Ref.[5]. $\alpha = 1$ is the Drude limit.
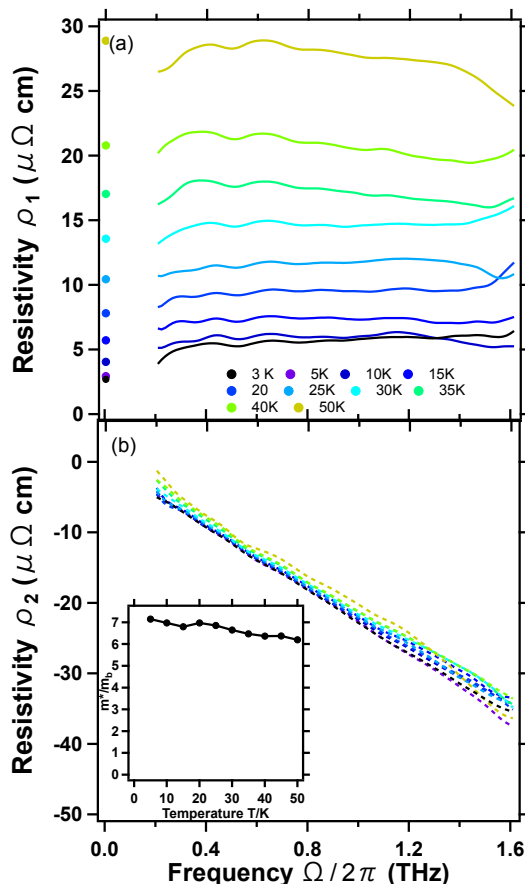
FIG. 6: (color online) (a,b) Real and imaginary parts of the complex THz resistivity at different temperatures. The real part of the resistivity is related to scattering rate while the slope of the imaginary part is a measure of the mass renormalization. The inset of (b) shows the frequency-averaged m^* as a function of temperature up to 50 K.

V. COMPLEX RESISTIVITY AND THE EXTENDED DRUDE ANALYSIS

Fig. S6 shows real and imaginary parts of complex optical resistivity calculated from inverting the conductivity. The real part of complex resistivity is plotted along with dc resistivity. The real part of resistivity ρ_1 at THz frequencies has only a weak frequency dependence, which is consistent with the scale of the relative contributions of temperature and frequency dependent scattering from the Gurzhi scaling[6]. At the lowest measured frequencies and low temperatures, there is a small drop in resistivity to the dc values, owing to the narrower Drude term. Nevertheless, we can still try to set bounds on the size of the ω^2 dependence to obtain an upper bound for the value of coefficient A from the general scaling relation $\rho_1(T,\omega) = \rho_0^{ee}(T)[1 + (\hbar\omega)^2/b\pi^2(k_BT)^2]$ where $\rho_0^{ee}(T)$ mentioned in the main text. In Fig. S7 we show the close up view of ρ_1 as plotted in Fig. 4(a) of the manuscript. The quadratic fits are presented as dashed black lines for different temperatures. Of the positive values, $b = 2.3$ for 5 K, $b = 5.5$ for 20 K, and $b = 7.7$ for 30 K, respectively. This is a size roughly consistent with Gurzhi scaling where $b = 4$ (the assumption that two particle Umklapp scattering dominates transport). Please note that the Gurzhi scaling implies that T dependent scattering will be larger than ω scattering and therefore at low frequencies disorder scattering will dominate over frequency dependent effects. This supports the notion that the scattering rate of each individual Drude feature is mostly frequency independent.

We performed extended Drude analysis, specifically to estimate its mass enhancement. The result is shown in the inset of Fig. S6 (b). Rewriting the complex conductivity $\sigma(\omega)$ in terms of a complex memory function, one obtains

$$\sigma(\omega) = \epsilon_0\omega_p^2 \frac{1}{1/\tau(\omega) - i\omega[1 + \lambda(\omega)]} \tag{4}$$

where, adopting Boltzmann-style terminology, $1/\tau(\omega)$ and $1 + \lambda(\omega)$ describe a frequency dependent scattering rate and mass enhancement (m^*/m_b) of the optical excitations due to many-body interactions[7]. Here $\omega_p/2\pi = 25,000$
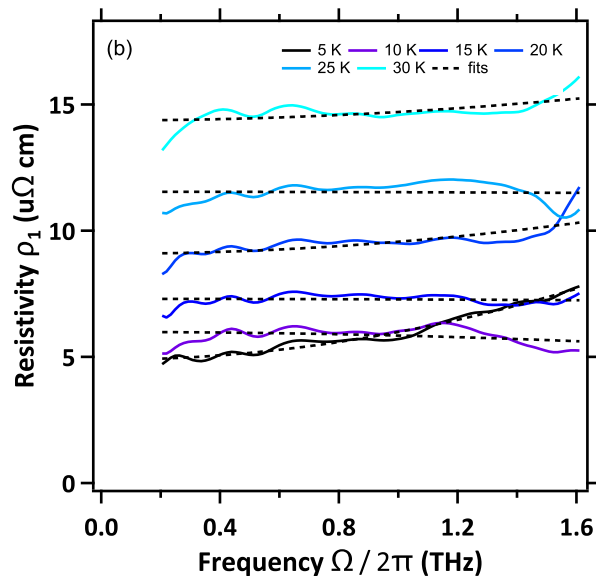
FIG. 7: Real part of the complex resistivity$\rho_1(\omega)$ and tentative quadratic fitting.

cm^{-1} is the plasma frequency from Ref.[8] and m_b is the effective band mass[9]. Equivalently, the imaginary part of the resistivity ρ_2 (Fig. S6(b)), can be used to estimate the magnitude of the effective mass by taking the slope of ρ_2 multiplied by $-\epsilon_0\omega_p^2$ (inset of Fig. S6(b)).
,

VI. ATTEMPTS AT MICROWAVE SPECTROSCOPY MEASUREMENTS

In the technique of Corbino broadband microwave spectroscopy[12], a coax cable connected to a network analyzer is terminated by a thin film sample (via a customized adapter that allows the sample to be press fit onto the end of the coax). Complex reflection coefficients are measured at each frequency of a scan, from which impedance can be calculated from the matching equations. A linear calibration scheme is used to obtain the actual reflection coefficient from the sample alone. In the thin film limit impedance can be inverted to obtain conductance. This technique is most sensitive when measuring samples that have impedances close to 50 Ω.

We attempted to measure thin films of SrRuO$_3$ in this technique's 10s of MHz to approximately 10 GHz range in order to partially fill in the missing frequency range between dc and the low end of the TDTS experiments. However these experiments proved to be very challenging. The issue is that the films are so highly conductive (impedances near 0.4 Ω) that their reflection coefficients are close to -1 making them hard to distinguish from a perfect conductor. In order to enhance the impedance of the highly conductive sample so that the reflection coefficient is farther from -1, the film is patterned into a thin strip geometry[13]. First a Au (200 nm)/Ti (5 nm) contact was evaporated on the sample using a macroscopic donut shaped (or Corbino) mask. Then the entire film was spin coated with about 2 microns of positive photo-resist and baked at 120° for 1 min to harden it. Afterwards, a thin strip mask, which was actually a thin Copper wire was attached to a glass slide (could be a micro-structure on photo mask), was aligned and pressed against the center of the donut shaped Au/Ti structure, and exposed to UV. The film was developed and rinsed with DI water, and re-baked for 1 min at 120°, so that a a thin strip (70 microns) of photo-resist was left on top of the sample. This strip made of photo-resist is then used as as a mask for Ar milling. The impedance was enhanced from this thin strip patterning by a factor of 22. Through this procedure, we attempted to measure the conductivity of thin strip samples.

Unfortunately, we believe that these efforts to measure the conductivity in this range largely failed. We always found a large and unexplained mismatch between THz and microwave data. Higher temperature (> 30 K) data was used as a substrate correction[12], assuming that the conductivity has a scattering rate much greater than 10 GHz according to extrapolation from THz data. However, it was found that the low temperature conductivity (especially < 20 K) exhibited a narrow Drude-like peak feature that was only of the order of a few GHz wide, which is much less than simple extrapolations of the THz to the dc conductivity. This result would imply a finite frequency peak in conductivity in the 50 GHz-150 GHz range. Although in principle this is possible, this would violate any simple

picture of extrapolating the THz data to the dc data and it is hard to envision any scenario in which this occurs. Moreover, such a scenario would give total spectral that that was strongly nonconserved as a function of temperature. Therefore we believe that this finite frequency peak is an artifact of still having a very low impedance and therefore considerable experimental uncertainty. Therefore, we could not reliably obtain the microwave conductivity, partly because the film is highly conductive and that contact impedance is difficult to model.

VII.   MODELING OF A TWO-BAND SYSTEM WITH PARABOLIC DISPERSION

The phenomenology of the crossover from two Drude peak-like conductivity at low temperature to a single Drude peak at higher temperature can be captured through a simple semiclassical model that captures the momentum non-conserving intraband scattering of individual bands and also the momentum conserving interband scattering between bands.

For a single-band Drude metal, the equation of motion is

$$-i\omega m v = qE - mv/\tau, \tag{5}$$

in which $-i\omega$ comes from the time derivative of the velocity, q is the charge (which can be e or $-e$) and τ is the average relaxation time of the velocity (proportional to current).

The velocity from this expression is then

$$v = \frac{qE\tau}{m}\frac{1}{1 - i\omega\tau}, \tag{6}$$

hence the complex ac Drude conductivity is

$$\sigma_{Dr} = \frac{nq^2\tau}{m}\frac{1}{1 - i\omega\tau}. \tag{7}$$

For a two-band system with parabolic dispersion, as discussed by Gantmakher[14], and Maslov and Chubukov[15], one can write down equations of motion that have a coupling between conduction channels due to interband electronic scattering. This interband non-current conserving (but momentum conserving) electron-electron scattering is represented with a friction coefficient η. This term has the effect of equalizing velocities between different conduction channels. The relaxation times τ_1 and τ_2, for the two bands take into account all non-momentum conserving (intraband and interband) scattering such as that that arises from disorder and umklapp scattering. Note that for parabolic bands, intraband momentum conserving electron-electron scattering, does not enter the equations of motion. The resulting expressions are

$$\begin{aligned}-i\omega m_1 v_1 &= q_1 E - m_1 v_1/\tau_1 - \eta n_2(v_1 - v_2), \\ -i\omega m_2 v_2 &= q_2 E - m_2 v_2/\tau_2 - \eta n_1(v_2 - v_1).\end{aligned} \tag{8}$$

These equations of motion result in interesting frequency dependent behavior, various limits of which are discussed in Ref.[15]. In the event that the metal is perfectly compensated $q_1 = -q_2$ and $n_1 = n_2$ then material is described by a single Drude-like peak at all frequencies. With excess of one charge species and even small momentum non-conserving scattering, then a two Drude structure appears with peaks whose widths are complicated functions of τ_1, τ_2, and η.

The issue we wish to address here is whether or not the conductivity given by these expressions is always given by a two Drude functional form (with of course highly effective scattering rates and densities). We find that it is, but that in various limiting cases and effective single Drude description suffices.

We define the following parameters and rewrite the equations for simplicity.

$$\begin{aligned}-i\omega m_1 v_1 &= q_1 E - \alpha_1 v_1 - \alpha_2 v_2, \\ -i\omega m_2 v_2 &= q_2 E - \beta_1 v_1 - \beta_2 v_2,\end{aligned} \tag{9}$$

in which

$$\begin{aligned}\alpha_1 &\equiv m_1/\tau_1 + \eta n_2 \\ \alpha_2 &\equiv -\eta n_2 \\ \beta_1 &\equiv -\eta n_1 \\ \beta_2 &\equiv m_2/\tau_2 + \eta n_1.\end{aligned} \tag{10}$$

Now let us make a new set of two equations which are independent linear combinations of the equations in 9. These will be equivalent to the Eqs. 9, and so are their solutions (see below for the constraints). Generically, one can use two different real dimensionless coefficients $c_{1,2}$. One multiplies the first equation by c_1 and adds it to the second, then multiplies the second equation by c_2 and adds it to the first. The new equations are

$$-i\omega(c_1 m_1 v_1 + m_2 v_2) = (c_1 q_1 + q_2)E - (c_1 \alpha_1 + \beta_1)v_1 - (c_1 \alpha_2 + \beta_2)v_2,$$
$$-i\omega(c_2 m_1 v_1 + m_2 v_2) = (c_2 q_1 + q_2)E - (c_2 \alpha_1 + \beta_1)v_1 - (c_2 \alpha_2 + \beta_2)v_2. \tag{11}$$

Note that the equivalency stated above necessitates constraints which are implicit in Eqs. 9 and 11. The Drude equation of motion (Eq. 5) is for a single particle and does not mention the density of electrons (which is proportional to the spectral weight). Moreover, the mass and charge of the carrier can be scaled by a common factor and the expression will stay the same. For the equation of motion, only the relaxation time τ is an essential parameter. A similar aspect exists for the two band coupled case. Transforming Eq. 9 to Eq. 11 requires implicitly, at least, that the spectral weight (or total charge) is unchanged.

Up to this point, we have not decoupled Eq. 9 and the expression for conductivity is not obvious. Nevertheless, we ask the following question: are there a set of coefficients, c_1 and c_2 that can put both equations in Eq. 11, in the same form as Eq. 5? If so, this implies that the complex ac conductivity can be written as a sum of two Drude-like terms. Here by "the same form", we mean that on the left-hand side of the equation, one has $-i\omega$ times a quantity that has the dimension of momentum, and on the right hand side of the equation, besides a charge times E term, one has the same momentum-like quantity, divided by a constant which only depends on material properties (specifically n_1, n_2, m_1, m_2, τ_1, τ_2, and η), but not on v_1, v_2, E, or ω. If there exists such c_1 and c_2, we have two equations which we know are equivalent to Eq. 9 and we know the solution (i.e. the form of conductivity) of. If c_1 and c_2 are different, these two equations are also independent of each other, i.e. the momentum-like quantities are not equal, $(c_1 m_1 v_1 + m_2 v_2) \neq (c_2 m_1 v_1 + m_2 v_2)$. Each of these momentum-like quantities contribute to the current, and therefore to conductivity. Therefore, the form of conductivity can be written as a sum of two Drude terms, although the spectral weight of either one is to be determined by conservation laws other than Eq. 11 itself. Apparently, there are numerous other arbitrary combinations of c_1 and c_2, but they do not decouple Eq. 9 in this manner and can not be solved independent of each other (although they are all equivalent equations to Eq. 9).

Now we seek such coefficients. If we find them, according to our argument above, we **can** write the conductivity as a sum of two Drude terms. In Eq. 5, the terms that includes the variable v are mv (momentum) on the left-hand side and mv/τ on the right-hand side. These two quantities differ by a factor which is τ and independent of v. Here in mapping to Eq. 5, we divide the corresponding quantities in the two equations of Eq. 11, respectively, which gives us

$$\frac{c_1 m_1 v_1 + m_2 v_2}{(c_1 \alpha_1 + \beta_1)v_1 + (c_1 \alpha_2 + \beta_2)v_2} \text{ and } \frac{c_2 m_1 v_1 + m_2 v_2}{(c_2 \alpha_2 + \beta_2)v_1 + (c_2 \alpha_2 + \beta_2)v_2} \tag{12}$$

Note that v_1 and v_2 depend on the steady state of the system and are independent variables. In general, the division will not be a constant, meaning they depend on v_1 and v_2, or in other words, the steady state of the system. Nevertheless, there is a particular situation, in which the division will cancel v_1 and v_2 in the numerator and denominator. The situation is when the coefficients for v_1 and v_2 have the same ratio in the numerator and denominator:

$$\frac{c_1 m_1}{c_1 \alpha_1 + \beta_1} = \frac{m_2}{c_1 \alpha_2 + \beta_2} \text{ and } \frac{c_2 m_1}{c_2 \alpha_1 + \beta_1} = \frac{m_2}{c_2 \alpha_2 + \beta_2}. \tag{13}$$

These ratios correspond to the relaxation time as in Eq. 5, (here we denote that τ for c_1 and c_2 as τ_a and τ_b, respectively, see Eq.16 below). This gives rise to a quadratic equation which have two solutions which correspond to two kinetic modes (Drude peaks)

$$m_1 \alpha_2 c_{1,\text{or } 2}^2 + (m_1 \beta_2 - m_2 \alpha_1)c_{1,\text{or } 2} - \beta_1 m_2 = 0. \tag{14}$$

The solution for the multipliers c is (one can show that the square root is always real, see below)

$$c_{1,2} = \frac{m_2 \alpha_1 - m_1 \beta_2 \pm \sqrt{(m_1 \beta_2 - m_2 \alpha_1)^2 + 4 m_1 \alpha_2 \beta_1 m_2}}{2 m_1 \alpha_2}$$
$$= \frac{m_1 m_2 (1/\tau_1 - 1/\tau_2) + \eta(m_2 n_2 - m_1 n_1) \pm \sqrt{(\eta(m_1 n_1 - m_2 n_2) + m_1 m_2 (1/\tau_1 - 1/\tau_2))^2 + 4\eta^2 m_1 m_2 n_1 n_2}}{-2\eta m_1 n_2} \tag{15}$$

Here we have found a particular choice of c_1 and c_2 which make the two quantities in Eq. 12 with no dependence on v_1 and v_2, which means if we plug the expressions in Eq. 15 back to Eq. 12, we obtain constants. That means the
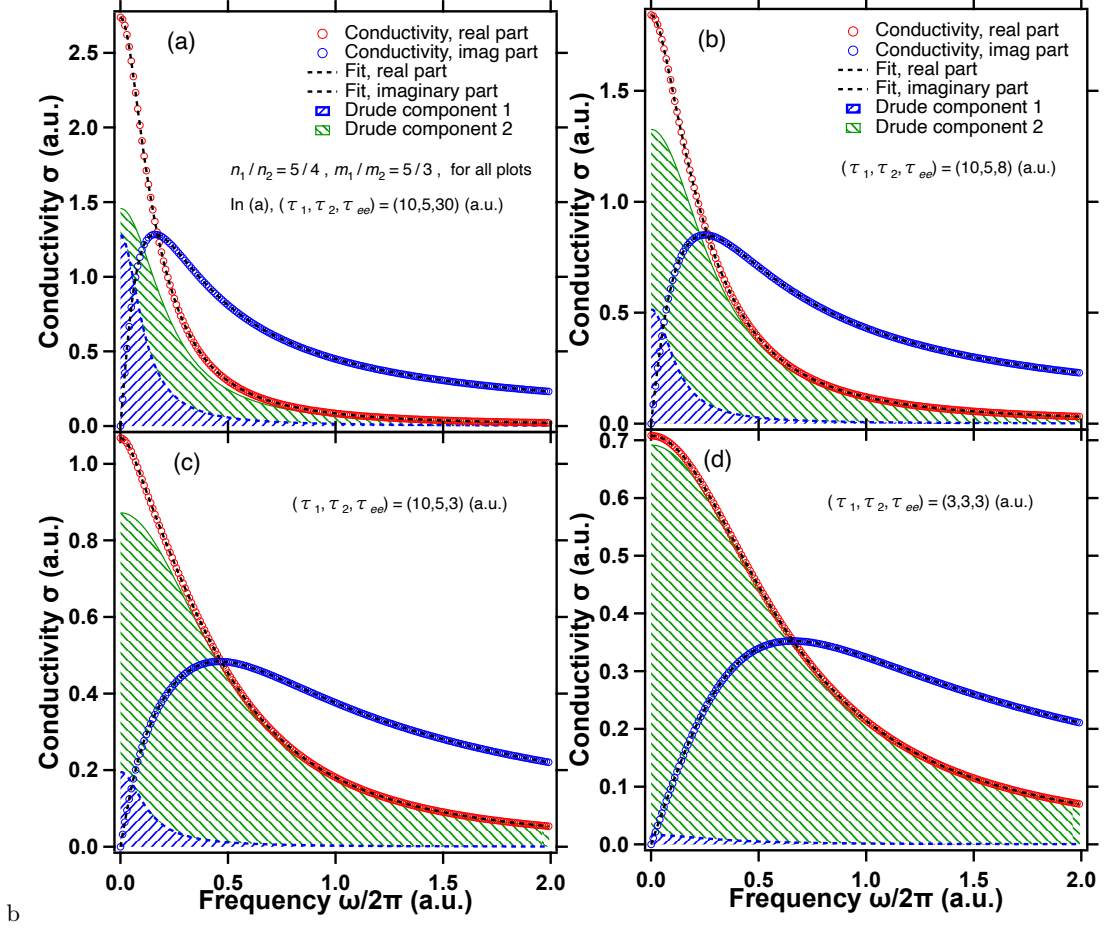
FIG. 8: Simulation of conductivity of the Maslov-Chubukov model using the parameters in the legends of each plot. The frequency and conductivity are in arbitrary units. The black dashed lines are two-Drude fits. One can see that as the interband electron-scattering increases then the relative contribution of the second peak decreases.

coefficients in Eq. 15 makes Eq. 11 correspond with the form of Eq. 5, and therefore we **can** write the solutions out since the Drude model solution is known (Eq. 7). Since this choice of c_1 and c_2 makes the two equations in Eq. 11 solvable separately without the need of the other equation, the equations in Eq. 9 are decoupled in this fashion.

Given the above real coefficients that do not depend on v_1, or v_2, one would be able to know the two relaxation times by plugging them back into Eq. 13, which we label as τ_a and τ_b, if using c_1 and c_2, respectively.

$$\tau_a = \frac{c_1 m_1}{c_1 \alpha_1 + \beta_1}, \tau_b = \frac{c_2 m_1}{c_2 \alpha_1 + \beta_1} \tag{16}$$

The charge of newly grouped carriers can just be defined as

$$q_a = c_1 q_1 + q_2, q_b = c_2 q_1 + q_2. \tag{17}$$

The definition of the new masses $m_{a,b}$ and new carrier densities $n_{a,b}$ should be in accordance with the conservation of total charge, total mass, and total momentum (based on the momemtum found in Eq. 13)

$$n_a q_a + n_b q_b = n_1 q_1 + n_2 q_2$$
$$n_a m_a + n_b m_b = n_1 m_1 + n_2 m_2 \tag{18}$$
$$n_a(c_1 m_1 v_1 + m_2 v_2) + n_b(c_2 m_1 v_1 + m_2 v_2) = n_1 m_1 v_1 + n_2 m_2 v_2.$$

The last equation of the three requires the coefficients for v_1 and v_2 to be equal since v_1 and v_2 depends on the steady state the system is in, and thus the following two equations.

$$n_a c_1 m_1 + n_b c_2 m_1 = n_1 m_1$$
$$n_a m_2 + n_b m_2 = n_2 m_2. \tag{19}$$

Through solving the above equations (which are obviously independent), one could obtain physically consistent effective masses, and carrier densities, for the two Drude terms. Specifically, one could use Eq. 19 to obtain n_a and n_b and plug into the first two equations of Eq. 18 to calculate m_a and m_b. Note that the conductivity depends on the ratio of n/m which means the choice for n and m is not unique. Here we have made the choice in Eq. 17 but in fact, the equations in Eq. 11 could be divided by any real constant, and therefore the definition of charge can be scaled up to a constant. But this does not change either conductivity or the scattering rate, or any physically measurable quantities.

Now, let us examine the scattering rates of the two Drude peaks in Eq. 13. The question is, if *assuming* all three scattering rates, $1/\tau_1$, $1/\tau_2$ and $1/\tau_{ee}$ (proportional to η) depends on temperature as T^2 (two-body scattering), do the two phenomological scattering rates $1/\tau_a$ and $1/\tau_b$ approximately scale as T^2? It is evident that all coefficients α_1, β_1, α_2, and β_2 scale as T^2 (at least in a *certain temperature range* where neither disorder nor phonon scattering dominates). Also note that $c_{1,2}$ are dimensionless constants which do not depend on temperature. Therefore, $1/\tau_a$ and $1/\tau_b$ according to the expression in Eq. 13, will scale as T^2. Nevertheless, with disorder scattering (say at very low temperatures), the constant term in the scattering rate, can be greater than T^2 and the result will be more complicated. Also, the mass and Fermi velocity of the two bands can be different, so the general temperature dependence does not need to be T^2, depending on the details of Fermi velocity, and electronic screening, etc.

What we have shown here is that despite the complicated lineshape given by the model in Refs.[14,15], it can always be decomposed into two Lorentzians. We demonstrate this in Fig. 8, where we show simulation of the model and a two-Drude model fitting. It can be seen that over the wide range of parameters demonstrated, a two-Drude model fits simultaneously the real and imaginary parts of the conductivity. In quite close correspondence to our data one can see that in the limit where the interband scattering is small (e.g. low temperatures), then the spectra are well-described by a two Drude fit. However at least for a situation close to compensation, the spectral weight of one of the these contributions gets smaller and smaller as the electron-electron interband scattering is increased (see Fig. 8(a-c)). For the compensated case[16,17], one can understand this in that for strong enough electron-electron scattering then the two otherwise independent channels are locked into a single effective one. See Fig. 8(d).

[1] H. P. Nair, Y. Liu, J. P. Ruf, N. J. Schreiber, S.-L. Shang, D. J. Baek, B. H. Goodge, L. F. Kourkoutis, Z.-K. Liu, K. M. Shen, et al., APL Materials **6**, 046101 (2018).

[2] D. B. Kacedon, R. A. Rao, and C. B. Eom, Applied Physics Letters **71**, 1724 (1997).

[3] F. Chu, Q. Jia, G. Landrum, X. Wu, M. Hawley, and T. Mitchell, Journal of Electronic Materials **25**, 1754 (1996), ISSN 0361-5235.

[4] A. Sushkov, G. Jenkins, D. Schmadel, N. Butch, J. Paglione, and H. Drew, Phys. Rev. B **82**, 125110 (2010).

[5] J. S. Dodge, C. P. Weber, J. Corson, J. Orenstein, Z. Schlesinger, J. W. Reiner, and M. R. Beasley, Phys. Rev. Lett. **85**, 4932 (2000).

[6] R. Gurzhi, Sov. Phys. JETP **8**, 673 (1959).

[7] A. V. Puchkov, D. N. Basov, and T. Timusk, Journal of Physics: Condensed Matter **8**, 10049 (1996).

[8] P. Kostic, Y. Okada, N. C. Collins, Z. Schlesinger, J. W. Reiner, L. Klein, A. Kapitulnik, T. H. Geballe, and M. R. Beasley, Phys. Rev. Lett. **81**, 2498 (1998).

[9] Note that this is a slightly smaller value than the 29100 cm^{-1} predicted from band structure calculations[10,11].

[10] I. I. Mazin and D. J. Singh, Phys. Rev. B **56**, 2556 (1997).

[11] I. I. Mazin and D. J. Singh, Phys. Rev. B **73**, 189903 (2006).

[12] W. Liu, *Broadband microwave measurements of two dimensional quantum matter* (PhD thesis, The Johns Hopkins University, 2013).

[13] M. Scheffler, S. Kilic, and M. Dressel, Review of Scientific Instruments **78**, 086106 (2007).

[14] V. Gantmakher and Y. Levinson, *Modern problems in condensed matter sciences Vol. 19: Carrier scattering in metals and semiconductors* (Elsevier–North-Holland, 1987).

[15] D. L. Maslov and A. V. Chubukov, Reports on Progress in Physics **80**, 026503 (2016).

[16] P. F. Maldague and C. A. Kukkonen, Physical Review B **19**, 6172 (1979).

[17] W. Baber, Proceedings of the Royal Society of London. Series A-Mathematical and Physical Sciences **158**, 383 (1937).